https://doi.org/10.1016/j.ijepes.2020.106153

Thermodynamic Modelling of Buried Transformer Substations for Dynamic Loading Capability Assessment Considering Underground Heat Accumulative Effect

Bin Zhou[a*], Xiaolin Xu[a], Siu Wing Or[b*], Canbing Li[a*], Qiuwei Wu[c*], Cong Zhang[a], Wenfang Li[d]

[a]*College of Electrical and Information Engineering, Hunan University, Changsha 410082, China*
[b]*Department of Electrical Engineering, The Hong Kong Polytechnic University, Hong Kong*
[c]*Department of Electrical Engineering, Technical University of Denmark, Lyngby 2800, Denmark*
[d]*Huaxiangxiangneng Electricity CO., LTD, Yiyang 413000, China*

Abstract

The lifetime cycle and secured service of buried transformers are constrained by their thermal insulation and loading conditions. This paper proposes an extended thermal circuit model for direct-buried transformer substations to dynamically evaluate the transformer loading capability. In the proposed model, the underground thermal interactions and energy balances among heat generation, transfer and storage in the transformer substation are represented with nonlinear thermal resistances and capacitances based on thermal-electrical analogies, and then hot-spot temperature (HST) dynamics can be captured from the nodal analysis on this R-C thermal equivalent circuit. Furthermore, the underground thermal accumulative effect is investigated for dynamic loading capability assessment considering the combined impact of heat accumulation in the surrounding soil caused by fluctuating transformer loads during prior operating periods. Finally, the finite element analysis with measured data is implemented for parameter tuning and model verification of the proposed thermodynamic model, and numerical simulations confirm the improvements of the proposed model for the transformer life extension and load management.

Highlights

A thermal circuit model for fully buried transformers is proposed to calculate the winding HST.
The underground heat accumulative effect is considered with soil thermal dissipation.
Dynamic assessment of loading capability is presented for transformer lifetime extension.
The finite element analysis is implemented for verification and tuning of the proposed model.

Keywords: Dynamic loading capability, hot-spot temperature, heat accumulative effect, thermal modelling, transformer.

* E-mail addresses of corresponding authors: licanbing@qq.com (C. Li), eeswor@polyu.edu.hk (S. W. Or), qw@elektro.dtu.dk (Q. Wu), binzhou@hnu.edu.cn (B. Zhou)

Nomenclature

Sets, Indices and Function

$f(x_j, \hat{\beta}_{(\alpha)})$	Observation equation of the jth sample
i	Index of time intervals
j	Index of samples on transformer HST
J_{total}	Total number of HST samples
N	Total number of time intervals
$S(\hat{\beta}_{(\alpha+1)})$	Sum of squared errors on HST
t_i	Time period at the ith iteration
$z_j(\hat{\beta}_{(\alpha)})$	First-order derivative of observation equation
α	Index of iteration number for nonlinear least-squares method
$\hat{\beta}_{(\alpha)}$	Current estimation of HST parameters at the αth iteration
ψ	Function of transformer thermal parameters
φ	Function of hydraulic resistance

Parameters

A	Heat dissipation area of transformer
B_1, B_2	Constants only determined by the type of the oil circulation
C_{cabin}	Thermal capacity of power distribution cabinet
C_{earth}	Thermal capacity from the outer casing of the substation to surrounding soils
C_{fan}	Thermal capacity of fans
C_{in}	Thermal capacity from the air in the substation to the outer casing of the substation
C_{oil}	Thermal capacity of transformer oil
C_{pump}	Thermal capacity of pumps
C_{tank}	Thermal capacity of transformer tank
C_{wnd}	Thermal capacity of transformer windings
D	Characteristic dimension, length, diameter or width
E	Aging rate constant
$F_{\text{AA},i}$	Aging acceleration factor during the ith time interval Δt_i
g	Gravitational constant
H_{cabin}	Height of power distribution cabinet
h	Heat transfer coefficient
K_{e}	Kersten number
k_{oil}	Oil thermal conductivity
L_{earth}	Thickness of underground soils involved in the heat transfer under the rated transformer loading
%LOL	Percent of transformer loss of life
m_{c}	Weight of core and coil
m_{oil}	Weight of transformer oil
$m_{\text{t,f}}$	Weight of transformer tank and fittings
m_{wnd}	Weight of transformer winding
P	Heat diffused by natural ventilations
R_{earth}	Soil thermal resistance
$R_{\text{hs-oil}}$	Thermal resistance from winding to oil
R_{hyd}	Hydraulic resistance
R_{in}	Thermal resistance from the air in the substation to the outer casing of the substation
R_{insul}	Thermal resistance of winding insulation
R_{oil}	Thermal resistance of transformer oil
R_{wnd}	Thermal resistance of winding
S	Surface of ventilation holes
T_{exp}	Transformer lifetime expectancy
T_{LOL}	Transformer LOL time
$T_{\text{LOL, IEEE}}$	LOL time determined by IEEE Loading Guide
T_{normal}	Normal insulation life of transformer
u, v, w	Coefficients indicating the nonlinearity between temperature rise and thermal resistance
λ_{sat}, λ_{dry}	Thermal conductivity of the saturated and dry soils respectively
λ_{s}	Effective thermal conductivity of soil solids
λ_{w}	Thermal conductivity of water
η	Soil porosity
γ_{oil}	Oil specific heat capacity
β_{oil}	Oil thermal expansion coefficient
ρ_{oil}	Oil density
ε_{oil}	Oil viscosity
δ	Oil texture dependent parameter
ω	Saturated rate of soil

Variables

q_{fe}, q_{cu}	Heat generated by core and copper losses
q_{sta}	Total heat generated by switch cubicles and boards
q_{tot}	Total heat generated by the substation
q_{tr}	Total heat generated by core and copper losses
$\mathbf{x_j}$	Input multi-point temperature vector measured by thermocouples
θ_{amb}	Ambient temperature
θ_{ex}	Temperature difference between inlet and outlet holes
θ_{hs}	Hot-spot temperature
$\theta_{\text{hs},j}$	Measured HST value of the jth sample
$\theta_{\text{hs,ref}}$	Reference hot-spot temperature
θ_{oil}	Top-oil temperature
θ_{sta}	Temperature of the air in the substation
$\Delta\theta_{\text{oil}}$	Top-oil temperature rise over the air in the substation
Δt_i	The ith time interval
$\boldsymbol{\mu_j}$	Error vector in the HST calculation of the jth sample

I. Introduction

A. Motivation

As an important link between the urban power network and consumers, the distribution transformer plays a significant role in ensuring a safe and reliable electricity supply for end-users. With the rapid growth of electrical load demand in urban agglomerations, the expansion of power distribution infrastructures is required for the installation or placement of new transformer substations [1]. Nevertheless, local authorities in large cities with high load densities become less and less tolerant on allocating scattered outdoor transformer substations in the public space, and overhead transformers also exhibit a negative visual impact on urban landscapes [2]. As the installation of power transformers is severely constrained with precious land resources in urban areas, the inappropriate location of substations would lead to the progressive increase of the cable waste and power network losses correspondingly [3],[4]. On the other hand, it has been reported in [5] that transformers inside buildings are likely to be less economic and would be associated with residential exposure to electromagnetic fields. Consequently, underground transformer substations, with the reductions on urban ground space, noise emissions and domestic electromagnetic radiations compared to conventional substations, are recognized as the cornerstone for the sustainability and urbanization of power distribution systems in recent years [6]-[8].

Underground transformer substations are generally electric distribution substations to convert the alternating current electricity from medium voltage to low voltage for residential and commercial applications, and they can be classified as semi-buried and direct-buried transformer substations [2]. The direct-buried transformer substation (DBTS) is a fully buried distribution substation inside the enclosure made of prefabricated metal or concrete materials, which is composed of a distribution transformer, low-voltage boards, medium-voltage cubicles, and other components [6]. Different from conventional overhead substations, the DBTS is surrounded by underground soils, and the heat caused by the core and copper losses of transformers should be dissipated by the oil cooling circulation and air ventilations inside the substation [9]. However, due to the soil thermal conductivity properties, the underground heat accumulation would be intensified so as to adversely increase the internal temperature of DBTS [10]. The excessive winding hot-spot temperature (HST) of buried transformers will give rise to the accelerated insulation aging with the loss of life (LOL) of transformers [11], and the performance degradation of winding insulations may even cause transformer failures along with distribution system blackouts [12],[13]. Moreover, since the transformer aging would be accelerated for the winding HST beyond a reference temperature of 110°C, the transformer loading capability non-linearly varies due to the changing HST [11],[14]. With the

continuous heat accumulation in the underground DBTS, the rated transformer loading cannot be tolerated when the transformer HST exceeds its threshold temperature [15]. Therefore, this research aims to investigate an extended thermal circuit model of direct-buried transformer substations for the dynamic loading capability assessment considering underground heat accumulative effects.

B. Relevant Background

So far, extensive studies on the modelling and operation of distribution transformer substations, such as thermal analysis and modelling [16]-[20], transformer LOL [21], transformer load management [22], insulation mediums and equipment [23],[24], ventilation and cooling systems [8],[9],[25], condition monitoring and fault diagnostics [12],[26]-[28], etc., have been investigated and tested with field experiments. As the HST is recognized as a critical criterion for governing the transformer's lifetime cycle and loading capability [29],[30], various methods have been developed to estimate the winding HST including empirical formulas [11],[28], direct measurements [14],[26], thermal circuit models [27],[30]-[33], and numerical analysis [9],[34]. Empirical formulas in the IEEE Loading Guide [28] have been widely used throughout the power industry. On the other hand, the direct measurement method for estimating HST behaviors by using fiber-optic sensors or thermocouple devices [26]. Nevertheless, it is difficult to determine the hot-spot location of transformers before installation, and the installed sensor is usually not located at the hottest hot-spot in many cases [28].

The thermal modelling methods adopt an equivalent thermal circuit based on thermal-electrical analogies proposed by Swift in [18] to capture different node temperatures of power transformers. Susa D et al. in [30],[31] added oil viscosity variations and loss changes with temperature into the thermodynamic model to calculate the HST, but the model in [30] only involves the oil thermal capacity without considering the thermal capacity of the windings, tank and core. Previous works in [19],[20],[33],[34] have investigated the thermal modelling of prefabricated indoor transformers, in which the thermal capacity and resistance of indoor transformers are different from those of outdoor transformers owing to the limited ventilations. Besides, the numerical-analytical technique based on finite element analysis was employed in [9],[35] as a thermal prediction tool to evaluate the hot-spot location and temperature distribution of transformers. The state-of-the-art research of the HTS calculation for transformer substations has been investigated in [8],[9],[29] with the combination of thermal circuit models and numerical finite element analysis. The natural convection of several underground DBTSs has been modelled numerically in [9] to analyze air flow patterns and temperature distribution inside the transformer substations, and a zonal thermal model is

further studied in [8] to promote and optimize the thermal characteristics of underground DBTSs. In summary, Table 1 lists and compares the differences of thermal models of transformer substations in various literatures. It can be found that, the thermal characteristics of soil surrounding underground transformers are not involved in the previous methods, and the underground thermal accumulative effect should also be considered due to the restricted ventilations compared with conventional overhead substations.

Table 1 Taxonomy of thermal modelling methods of transformer substations

Reference	Object	Modelling method	Dynamic loading capability assessment	Underground thermal accumulative effect
[7]	Underground transformer	Thermal circuit models	×	×
[8]	Underground transformer substations	Thermal models + Numerical analysis	×	×
[9]	Underground transformer substations	Numerical analysis	×	×
[17]	Direct buried transformer	Empirical formulas	×	×
[34]	Prefabricated transformer substations	Thermal circuit models + Numerical analysis	×	×
This paper	Direct buried transformer substations	Thermal circuit models + Numerical analysis	√	√

The life expectancy of a transformer is the normal transformer service life under the rated loading, and it can be determined by the transformer LOL, which is the equivalent aging in hours at the reference HST in a given time period for an actual temperature cycle [21]. The transformer loading capability should be dynamically assessed to determine the maximum allowable loading which this transformer can acceptably sustain under the time-varying loading and environmental conditions [28]. Once the transformer load seriously exceeds this loading capacity, the demand response or load shedding can be performed to decrease the transformer LOL for lifetime extension. Most of the existing approaches for dynamic loading capability assessment are carried out through a thermal circuit model in [14],[15] with empirical data from air temperature and current measurements. In addition, a flowchart of self-consistent time-dependent mathematical model is proposed in [29] to determine the transformer loading capability. In general, the IEEE Loading Guide in [11] provides a classical method for loading capability assessment based on the average winding test temperature rise. It should be noted that, due to the soil thermal dissipation with thermal lags in the HST rise of underground transformers, the dynamic loading capability assessment should consider the impact of heat accumulation in the surrounding soil caused by fluctuating transformer loads during prior operating periods.

C. Contribution and Organization of the Paper

This paper is devoted to exploiting thermal characteristics of the buried transformers in underground substations, and further investigating the dynamic loading capacity assessment of DBTS with the proposed thermodynamic model. The major contributions of this research are outlined follows: 1) An extended thermal circuit model is proposed to dynamically calculate the winding HST of DBTS, and the finite element analysis with measured data is further implemented to analyze the temperature distribution of DBTS for verification and tuning of the proposed model; 2) The underground thermal accumulative effect on the HST of fully buried transformers caused by soil thermal properties is discovered and verified through numerical simulations; 3) An iterative approach for dynamic loading capacity assessment based on the proposed thermal circuit model is formed to increase the service life of transformer.

The remainder of this research is organized as follows: the architecture and thermodynamic modelling of DBTS are formulated and investigated in Section II. In Section III, the underground heat accumulative effect is studied and the dynamic loading capability is evaluated based on the proposed thermal circuit model. The finite element analysis is further implemented for verifying and tuning the proposed model, and comparative case studies are implemented and analyzed in Section IV. Finally, concluding remarks are drawn in the last Section.

II. Thermodynamic Modelling of DBTS

A. Architecture of DBTS

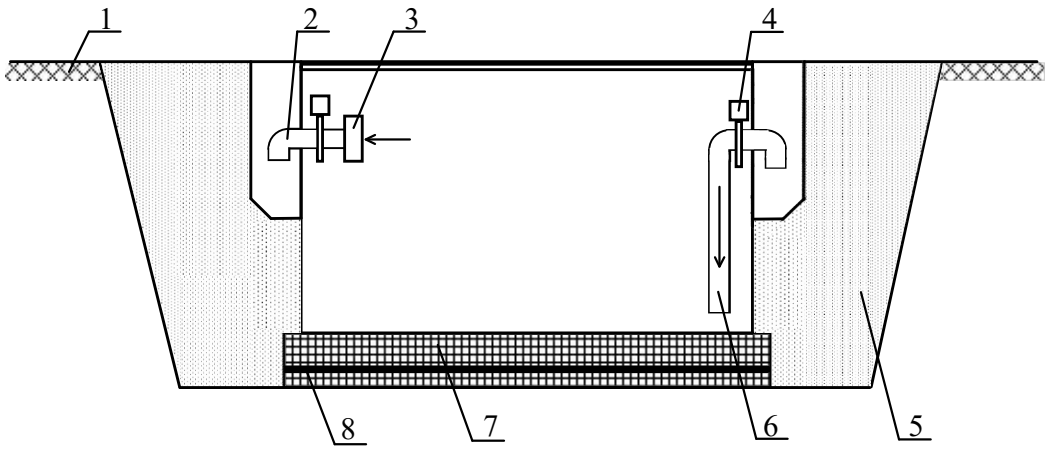

1-Ground level **2**-Output ventilation holes **3**-Axial flow fan **4**-Electronic butterfly valve
5-Soil **6**-Input ventilation hole **7**-Foundation **8**-Embedded steel plate

Fig. 1 Overall architecture of DBTS

As shown in Fig. 1, the DBTS is lifted into the prefabricated underground pit with lifting equipment and also fixed with anchor bolts. Besides, the transformer cabinet needs to be effectively grounded. The DBTS is composed of a buried cabinet, a distribution transformer, low-voltage boards, medium-voltage cubicles and other components [8],[9] as depicted in Fig. 2. The oil-immersed power transformer adopted in this paper has the rated capacity of 630kVA [36]. Rated voltage for primary winding and secondary winding in the transformer are 10±2×2.5% kV and 0.4kV, respectively. Meanwhile, metal-enclosed SF_6 insulated switchgear is used in the medium-voltage cubicles.

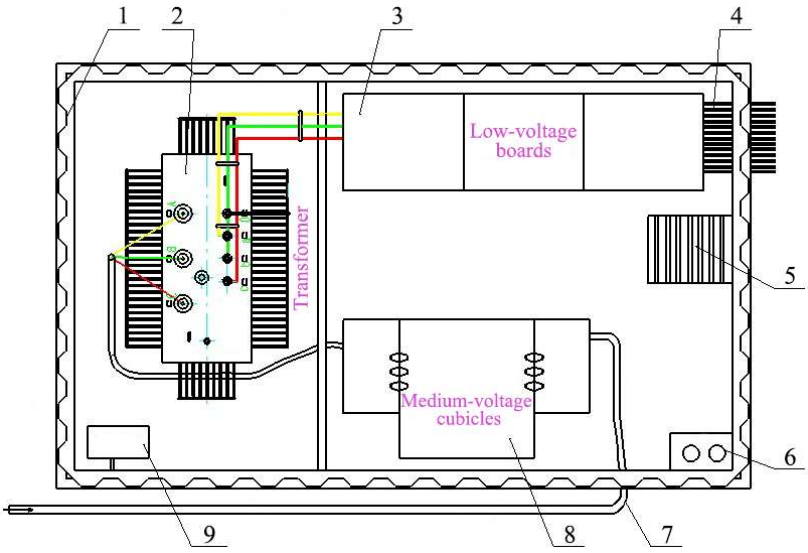

(a)

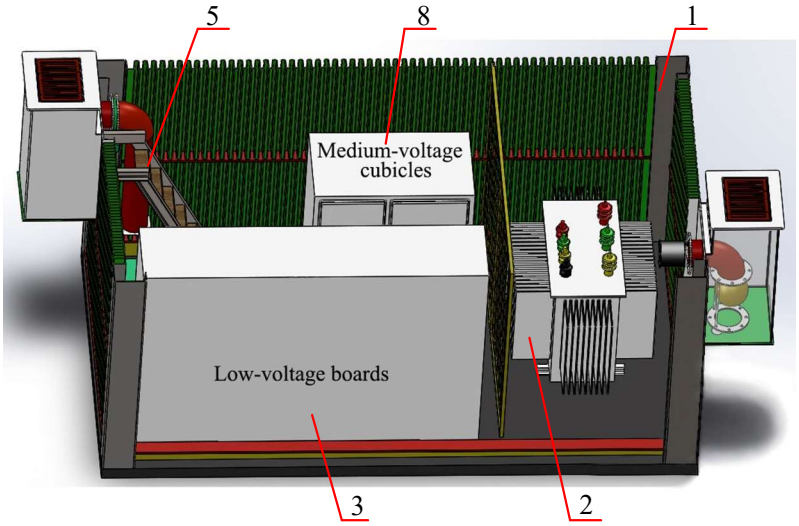

(b)

1-Tank **2**-Transformer **3**-Low-voltage boards **4**-Outgoing distribution cables **5**-Movable stair **6**-Fire extinguisher **7**-Incoming local transmission cables **8**-Medium-voltage cubicles **9**-Immersible pump

Fig. 2 Internal structure and layout of DBTS

B. Extended Thermal Circuit Model

Traditional methods in [18]-[20] for the temperature-rise analysis of transformers generally adopt the basic thermal circuit model derived from the thermal-electrical analogy. As shown in Table 2, the thermal-electrical analogy can be defined as applying electrical principles in the electric circuit to the thermal circuit [18], and the thermal resistance and capacity are defined as the cabinet material's ability to resist heat flow and store heating energy [37]. Here, the across variable is referred as a variable whose value can be measured by a difference of the values at two extreme points of an element, and the through variable is defined as a variable transmitted through an element in the thermal and electrical circuits [20].

Table 2 Thermal-electrical analogous quantities

Variables	Thermal circuit	Electrical circuit
Across variable	Temperature, θ, ℃	Voltage, v, V
Through variable	Transferred power, q, W	Current, i, A
Storage element	Thermal capacitance, C_{ch}, J/℃	Elec. capacitance, C_{el}, F
Dissipation element	Thermal resistance, R_{th}, ℃/W	Elec. resistance, R_{el}, Ω

Fig. 3 shows a typical model proposed by Susa for outdoor transformers [30]. With the thermal circuit models in Fig. 3, the value of θ_{oil} obtained from the top-oil temperature (TOT) model can be substituted into the HST model to solve the value of θ_{hs}. Here, q_{tot} is the sum of q_{cu} and q_{fe}.

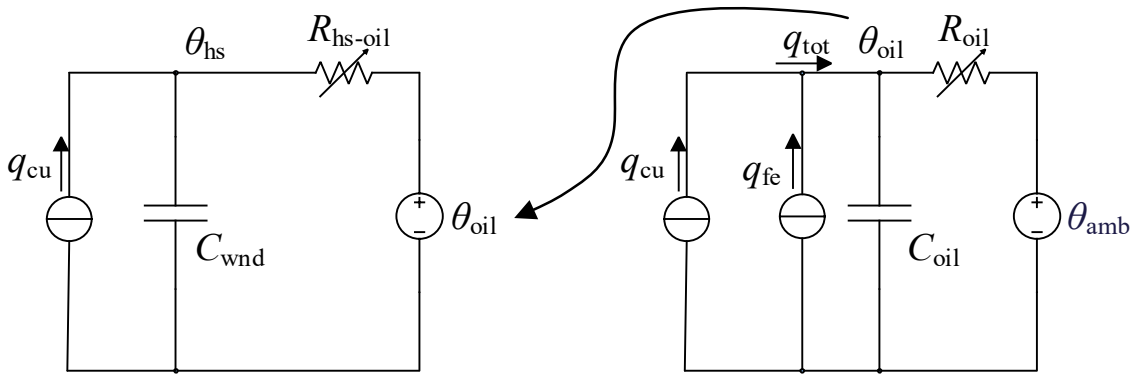

(a) HST model (b) TOT model

Fig. 3 Basic transformer thermal circuit model

Due to the underground heat accumulative effects, the basic thermal circuit model in Fig. 3 cannot be applicable for DBTS, and the underground thermal interactions and energy balances among heat generation, transfer and storage should be considered to form the underground transformer thermal circuit model. Consequently, this research proposes an extended thermal circuit model for DBTS with the thermal capacity

and resistance of the underground soil involved in heat dissipation. In the proposed thermal circuit model, the outermost layer ambient temperature is set to the average soil temperature, and the extended thermal circuit can be derived from the energy balances for transformer windings, iron cores, transformer tank and oil, medium-voltage cubicles, low-voltage boards, cooling air inside the substation, other equipment in the substation, substation cabinet and surrounding soils.

In the extended model in Fig. 4, the left side of the dotted line in the model is the internal structure of the transformer, and the right side is the structure of external environment. Here, the heat sources consist of the inner transformer power loss and the heat generated by distribution cabinets. The heat also dissipates from iron cores and windings to oil, from oil to air in the substation, and from air to external soil. For the TOT model in Fig. 4(b), the heat generated by DBTS can be regarded as ideal current sources. A part of the heat is absorbed by C_{oil}, C_{in} and C_{earth}, and another part acts as a heat source to cause temperature rises of transformer oil and air in the substation. The rest diffuses into the external environment by R_{oil}, R_{in} and R_{earth}. Besides, the ambient temperature can be modelled as an ideal voltage source. It should be noted that the heat generated by stray losses can be ignored since the equivalent thermal resistance of stray parts is less than 5×105 K/W [19].

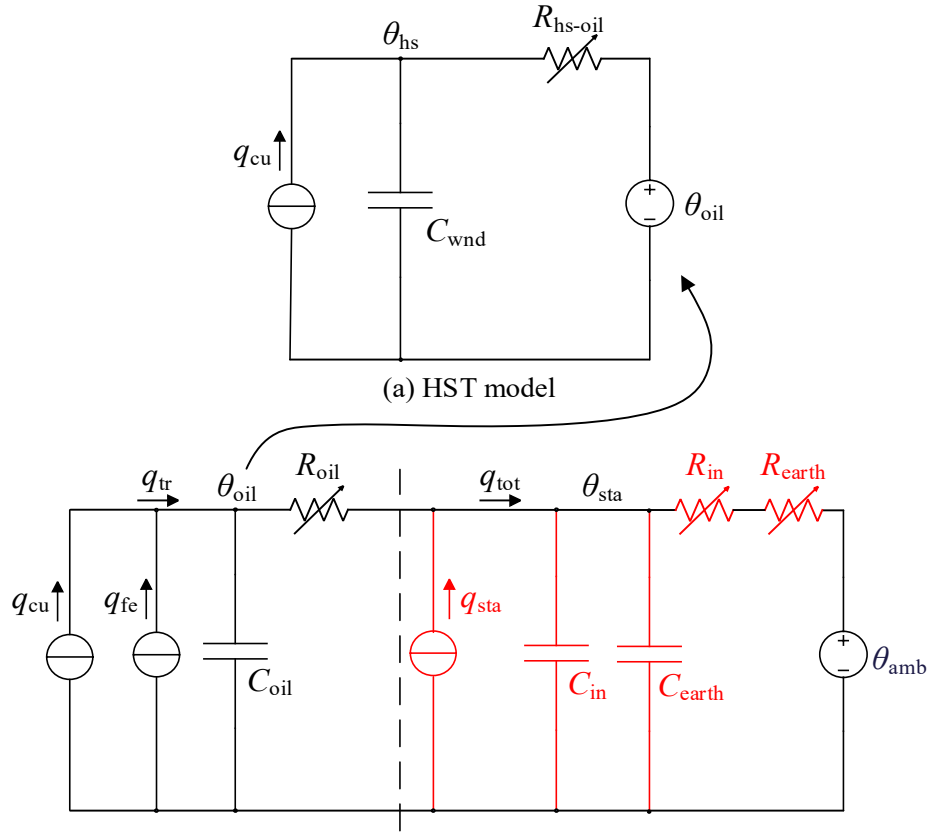

Fig. 4 Extended thermal circuit model of DBTS

Moreover, the value of q_{tot} in the TOT model can be calculated from the sum of q_{cu}, q_{fe} and q_{sta}. Here, the value of q_{sta} is determined by the product of the actual load factor and the total amount of heat dissipation from switch cubicles and boards under the rated transformer load, and the rated heat dissipation of switch cubicles and boards are listed in Table 7.

C. Parameter Tuning and Analysis

1) Thermal capacity and resistance of transformer

Taking the oil-immersed transformer as the typical example, the equivalent thermal resistance R_{oil} can be obtained by the following formula:

$$R_{\text{oil}} = \frac{\Delta\theta_{\text{oil}}}{q_{\text{tr}}} = \frac{1}{h \times A} \tag{1}$$

Since the transformer oil thermal resistance is not constant when the temperature changes, it is necessary to define the relevant nonlinear thermal resistance expression. Eq. (2) can be obtained by using Grashof number, Prandtle number and Nusselt number [20]:

$$\frac{h \times D}{k_{\text{oil}}} = B_1 \times [(\frac{\gamma_{\text{oil}} \times \varepsilon_{\text{oil}}}{k_{\text{oil}}}) \times (\frac{L^3 \times \rho_{\text{oil}}^2 \times g \times \beta_{\text{oil}} \times (\Delta\theta_{\text{oil}})}{\varepsilon_{\text{oil}}^2})]^{B_2} \tag{2}$$

where B_1 and B_2 can be obtained from Table 3 [19].

Table 3 Empirical values for parameters B_1 and B_2

Oil circulation type	B_1	B_2
Turbulent	0.10	0.33
Laminar	0.59	0.25

The variations of thermal parameters with respect to temperature is given in Table 4 [19]:

Table 4 Temperature function of transformer thermal parameters

Parameter	Symbol	Temperature function
Oil density	$\rho_{\text{oil}}(\theta)$	$1098.72\text{-}0.712\theta$
Oil thermal conductivity	$k_{\text{oil}}(\theta)$	$0.1509\text{-}7.101\times10^{-0.5}\theta$
Oil specific heat capacity	$\gamma_{\text{oil}}(\theta)$	$807.163+3.5\theta$
Oil thermal expansion coefficient	$\beta_{\text{oil}}(\theta)$	8.6×10^{-4}
Oil viscosity	$\varepsilon_{\text{oil}}(\theta)$	$0.08467\text{-}0.0004\theta+5\times10^{-7}\theta^2$

It can be seen from Table 4 that, the change of the oil viscosity with temperature is significantly higher than those of other thermal parameters. To simplify the model, this study approximate thermal parameters, except for the viscosity, to constant functions of temperature [30]. Then, Eq. (2) can be rewritten as:

$$h = \psi \times (\frac{\Delta\theta_{\text{hs}}}{\varepsilon_{\text{oil}}(\theta)})^{B_2} \tag{3}$$

where ψ can be obtained in Eq. (4) and then is set as a constant:

$$\psi = B_1 \times [\rho_{\text{oil}}^2 \times g \times \beta_{\text{oil}} \times k_{\text{oil}}^{(\frac{1-B_2}{B_2})} \times L^{(\frac{3B_2-1}{B_2})} \times \gamma_{\text{oil}}]^{B_2} \tag{4}$$

The thermal capacity of oil can be obtained according to the empirical formula given in the IEEE Loading Guide [11]:

$$C_{\text{oil}} = 0.1323 m_{\text{c}} + 0.0882 m_{\text{t,f}} + 0.400 m_{\text{oil}} \tag{5}$$

$$C_{\text{oil}} = 0.1323 (m_{\text{c}} + m_{\text{t,f}}) + 0.580 m_{\text{oil}} \tag{6}$$

Here, Eq. (5) is suitable for oil-immersed self-cooled transformers and Eq. (6) is suitable for oil-immersed transformers.

The nonlinear thermal resistance from transformer windings to oil can be obtained by the following formula [30]:

$$R_{\text{hs-oil}} = R_{\text{wnd}} + R_{\text{insul}} + R_{\text{oil}} \tag{7}$$

The relation among R_{wnd}, R_{insul} and R_{oil} is given in Eq. (8). Thus, Eq. (7) can be simplified as Eq. (9) and the formula for heat transfer factor h can be given in Eq. (10),

$$\begin{cases} R_{\text{oil}} >> R_{\text{wnd}} \\ R_{\text{oil}} >> R_{\text{insul}} \end{cases} \tag{8}$$

$$R_{\text{hs-oil}} = R_{\text{oil}} = \frac{1}{h \times A} \tag{9}$$

$$h = \psi \times (\frac{\Delta\theta_{\text{hs}}}{\varepsilon_{\text{oil}}(\theta)})^{B_2} \tag{10}$$

It should be noted that the viscosity $\varepsilon_{\text{oil}}(\theta)$ here should be evaluated again at the TOT and $\Delta\theta_{\text{hs}}$ is now the winding temperature rise over the top-oil. The thermal capacity of the windings can be obtained from Eq. (11):

$$C_{\text{wnd}} = 0.132 m_{\text{wnd}} \tag{11}$$

2) Thermal capacity and resistance inside substation

The thermal resistance inside the substation refers to the thermal resistance of the path, through the heat is transferred from the outer surface of the equipment in the substation (transformer tank, low-voltage boards, medium-voltage cubicles, etc.) to the substation enclosure. Also, air inside the substation is mainly cooled by natural ventilations, which can be represented by the thermal resistance R_{in}. The value of R_{in} can be derived from the Hoppner formula [33]:

$$S = \sqrt{\frac{13.2P^2 R_{\text{hyd}}}{\theta_{\text{ex}}^3 H_{\text{cabin}}}} \tag{12}$$

Here, it is assumed that the surface of input ventilation holes is equal to output ventilation vents. Take P as an unknown variable and Eq. (12) can be rewritten as:

$$P = \varphi \theta_{\text{ex}}^{1.5} \tag{13}$$

$$\varphi = S\sqrt{\frac{H_{\text{cabin}}}{13.2R_{\text{hyd}}}} \tag{14}$$

The relationship between θ_{ex} and R_{in} can be obtained from $\theta_{\text{ex}} = R_{\text{in}} \times P$ and Eq. (13) can be modified as:

$$R_{\text{in}} = \frac{1}{\varphi \theta_{\text{ex}}^{0.5}} \tag{15}$$

where, the value of φ is usually obtained from experiments:

$$\varphi = 64.899 \times (1 - e^{-5.37S}) \tag{16}$$

The thermal capacity inside the substation reflects the heat storage capacity of the equipment in the substation and the air inside the substation. The thermal capacity of the air can be ignored because it is much smaller than the thermal capacity of the equipment, as follows:

$$C_{\text{in}} = C_{\text{tank}} + C_{\text{fan}} + C_{\text{pump}} + C_{\text{cabin}} \tag{17}$$

Here, the specific heat capacity of each component can be estimated by C=0.22m, i.e. the product of the specific heat and mass [20].

3) Thermal capacity and resistance outside substation

The heat dissipation capacity of the soil is mainly reflected in its thermal resistance, that is, the thermal conductivity of the soil. It is affected by factors such as soil composition, temperature, moisture and porosity. The thermal resistance of soil around buried substation is estimated by Johansen model [38]:

$$R_{\text{earth}} = \frac{L_{\text{earth}}}{(\lambda_{\text{sat}} - \lambda_{\text{dry}})K_{\text{e}} + \lambda_{\text{dry}}} \tag{18}$$

where L_{earth} can be obtained from the simulation results; K_{e}, λ_{sat}, λ_{dry} can be obtained from Eq. (19)-(21):

$$K_{\text{e}} = \text{e}^{\delta[1-\omega^{\delta-1.33}]} \tag{19}$$

$$\lambda_{\text{sat}} = \lambda_{\text{s}}^{1-\eta} \cdot \lambda_{\text{w}}^{\eta} \tag{20}$$

$$\lambda_{\text{dry}} = -0.56\eta + 0.51 \tag{21}$$

Soil parameters adopted in this paper are shown in Table 5. The specific heat of the soil is related to the amount of water and air involved. The soil specific heat capacity here is taken as 1645 J/ (kg °C).

Table 5 Thermal parameters of soil

Soil texture	δ	ω	η	λ_s	λ_w
Loam	0.9	0.6446	0.3	3.62	0.594

It should be noted that some coefficients from Eq. (3)-(21), such as soil thermal capacity and resistance, would vary with the surrounding soil environment and their own physical characteristics. For instance, the soil thermal capacity and resistance are affected by the soil moisture and temperature, while the transformer oil thermal resistance is affected by the top-oil temperature rise over the air in the substation. Compared with traditional overhead substations, the parameters of DBTS have less uncertainties due to the slowly varying soil properties including the soli ambient temperature and moisture. Consequently, these model parameters need to be recalibrated monthly based on the experimental measurement results in [39].

4) Mathematical expression of buried transformers

The HST can be calculated from the sum of the external soil temperature, the air temperature rise in the substation over the soil, the top-oil temperature rise over air in the substation, and the windings temperature rise over the top-oil. The differential form of the proposed thermal circuit model is expressed as the following three parts, as follows:

$$q_{cu} = C_{wnd}\frac{d\theta_{hs}}{dt} + \frac{1}{R_{hs\text{-}oil}}[\theta_{hs} - \theta_{oil}]^{1/u} \tag{22}$$

$$q_{fe} + q_{cu} = C_{oil}\frac{d\theta_{oil}}{dt} + \frac{1}{R_{oil}}[\theta_{oil} - \theta_{sta}]^{1/v} \tag{23}$$

$$q_{fe} + q_{cu} + q_{sta} = (C_{in} + C_{earth})\frac{d\theta_{sta}}{dt} + \frac{1}{R_{in} + R_{earth}}[\theta_{sta} - \theta_{amb}]^{1/w} \tag{24}$$

where $1/u$, $1/v$ *and* $1/w$ reflect the nonlinearity between temperature rise and thermal resistance. The heat generated by the transformer core and copper losses can be estimated by the factory test or operating data of the transformer. Thermal capacity and resistance, nonlinear coefficient and the total heat generated by the buried substation except the core and copper losses can be derived from experience.

After inputting the ambient temperature and operating data of underground transformers, the first-order differential Eq. (24) can be solved to obtain the temperature rise of air in the DBTS. Then, temperature rises of the transformer oil and the hot-spot can be obtained by Eq. (23) and Eq. (22). Therefore, the winding HST can be further solved to determine whether underground transformers temperature rise can meet

requirements for safe operations. If not, the load management should be adopted.

5) Parameter tuning with nonlinear least-squares method

The nonlinear least-squares method [15] is used to tune the soil thermal capacity and resistance based on measured data under different load factors of DBTS. The functional relationship between measured values ($\mathbf{x_j}, \theta_{\mathrm{hs},j}$) and the observation equation $f(\mathbf{x_j}, \hat{\beta}_{(\alpha+1)})$ is given in Eq. (25), and the sum of squared errors is defined in Eq. (26):

$$\theta_{\mathrm{hs},j} = f(\mathbf{x_j}, \hat{\beta}_{(\alpha)}) + \boldsymbol{\mu_j} \tag{25}$$

$$S(\hat{\beta}_{(\alpha+1)}) = \sum_{j=1}^{J_{total}} (\theta_{\mathrm{hs},j} - f(\mathbf{x_j}, \hat{\beta}_{(\alpha+1)}))^2 \tag{26}$$

A first-order Taylor series of $f(\mathbf{x_j}, \hat{\beta}_{(\alpha+1)})$ is employed by Gauss-Newton algorithm to approximate $f(\mathbf{x_j}, \hat{\beta}_{(\alpha+1)})$ as shown in Eq. (27), where $z_j(\hat{\beta}_{(\alpha)})$ is defined in Eq. (28). Then, the minimization problem described in Eq. (26) is reduced to a linear least-squares problem as shown in Eq. (29) [15]. Moreover, the parameters of the next iteration can be obtained in Eq. (30):

$$f(\mathbf{x_j}, \hat{\beta}_{(\alpha+1)}) \approx f(\mathbf{x_j}, \hat{\beta}_{(\alpha)}) + \frac{df(\mathbf{x_j}, \hat{\beta}_{(\alpha)})}{d\hat{\beta}_{(\alpha)}} (\hat{\beta}_{(\alpha+1)} - \hat{\beta}_{(\alpha)}) \tag{27}$$

$$z_j(\hat{\beta}_{(\alpha)}) = \frac{df(\mathbf{x_j}, \hat{\beta}_{(\alpha)})}{d\hat{\beta}_{(\alpha)}} \tag{28}$$

$$\min \left\| \theta_{\mathrm{hs}} - f(\mathbf{x}, \hat{\beta}_{(\alpha)}) - z(\hat{\beta}_{(\alpha)})(\hat{\beta}_{(\alpha+1)} - \hat{\beta}_{(\alpha)}) \right\|_2^2 \tag{29}$$

$$\hat{\beta}_{(\alpha+1)} = \hat{\beta}_{(\alpha)} + (z_{(\alpha)}^{\mathrm{T}} \cdot z_{(\alpha)})^{-1} \cdot z_{(\alpha)}^{\mathrm{T}} \cdot (y_j - f(\mathbf{x_j}, \hat{\beta}_{(\alpha)})) \tag{30}$$

Here, the value of $\hat{\beta}_{(\alpha+1)}$ obtained in Eq. (30) shall be regarded as $\hat{\beta}_{(\alpha)}$ in the next iteration. Then, Eq. (27)-(30) should be repeatedly recalculated based on the updated value of $\hat{\beta}_{(\alpha)}$ to obtain the new $\hat{\beta}_{(\alpha+1)}$ until the change of β is below a threshold value (set to be 10^{-8} in this study).

III. Impacts of Heat Accumulative Effect on Dynamic Loading Capability

A. Heat Accumulative Effect

For validating the heat accumulative effect presented in Section II, this paper adopts the data of load factor from the IEEE Loading Guide [11] to simulate thermal behaviors of transformer HST, and then further compare and analyze the calculation results. Fig. 5 provides the transformer HST trajectory with the variations of load factor.

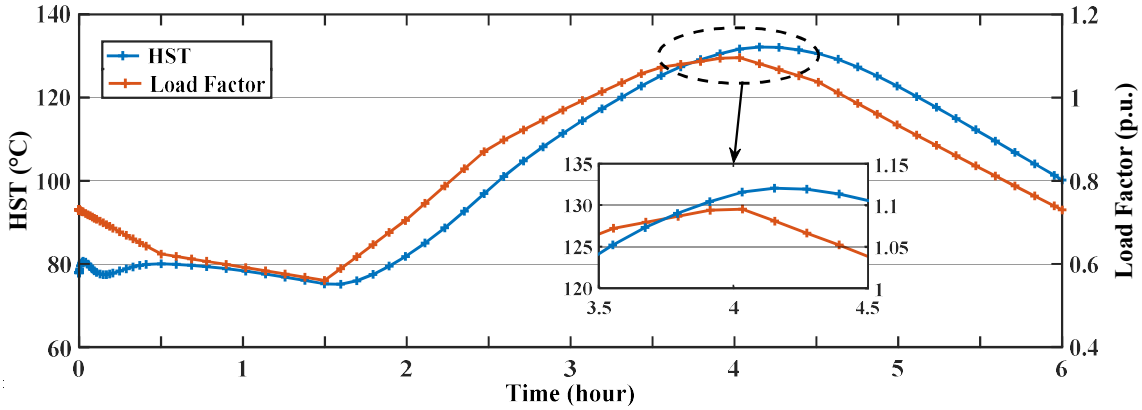

Fig. 5 Verification of heat accumulative effect

From the Fig.5, it can be found that the variation of the HST is not consistent with the load factor. When the transformer load suddenly decreases at hour 4, the HST maintains the same or even increases for about half hour. Similarly, when the load suddenly increased at hour 1.5, the response time of the HST is postponed. The underground heat accumulation effect is a thermodynamic phenomenon expressed as the changes to internal temperatures in the DBTS caused by the combined influences of heat generated by past and present transformer load. Consequently, it can be discovered that the heat accumulation effect in the underground direct-buried pit would postpone the temperature response to the transformer load. Compared with the outside air around conventional overhead substations, the thermal capacity of the soil around the underground transformer is significantly higher than that of the ambient air, and the thermal capacity plays an important role for the underground heat storage and accumulation during the heat diffusion process. Also, the soil thermal resistance will slow down the rate of the heat diffusion from the transformer windings to the external environment. Both of the thermal capacity and resistance will delay the response time as well as reduce the HST variation in magnitude. Therefore, the calculation of the HST should be combined impact of heat accumulation in the surrounding soil caused by fluctuating transformer loads during prior operating periods. The proposed thermal circuit model in Fig. 4 and differential equations in Eq. (22)-(24) are then employed to calculate the dynamical HST in the underground substation.

B. Dynamic Loading Capability Assessment of DBTS

Dynamic loading capability assessment is to identify the maximum amount of the electrical load that the transformer winding insulation can tolerate in excess of the capacity rating. The winding temperature is recognized as the most important factor to affect the thermal insulation aging of transformers, as the overloading temperature will cause the insulation materials to release gas bubbles and may even result in irreversible insulation failure [24]. On the other hand, since the temperature is maldistribution in multi-

phase transformer windings, the hottest spot temperature is usually used to evaluate the insulation aging of transformers [26]. Based on Arrhenius reaction rate theory in [11], the aging acceleration factor F_{AA} can be given as,

$$F_{AA} = \mathrm{Exp}\left(\frac{E}{\theta_{hs,ref} + 273} - \frac{E}{\theta_{hs} + 273}\right) \tag{31}$$

where $\theta_{hs,ref}$ is defined as the temperature at which the transformer can continue to operate for the entire normal life cycle [31]. For the HST values beyond the reference HST, this aging acceleration factor should be larger than 1. Otherwise, this factor should be lower than 1. The determination on the value of reference HST should consider the transformer normal lifetime. In this study, based on the standard normal lifetime of 180000 hours used in the DBTS, the reference HST is set as 110 °C from the results of functional life testing provided in [11]. Also, the aging rate constant E is influenced by mechanical characteristics of transformers, such as burst strength, tensile strength and elongation to rupture, and its value can be derived by the per unit transformer insulation life curve in [36]. Here, the aging rate constant is set to 15000 for the studied distribution transformer in this case study.

For a given time period with temperature cycles, the LOL time, the percent of transformer LOL, and the transformer lifetime expectancy can be expressed by Eq. (32)-(34), as follows,

$$T_{LOL} = \sum_{i=1}^{N} F_{AA,i}\,\Delta t_i \tag{32}$$

$$\%\,\mathrm{LOL} = \frac{T_{LOL}}{T_{normal}} \times 100\% \tag{33}$$

$$T_{exp} = T_{normal} \times \frac{T_{LOL,\,IEEE}}{T_{LOL}} \tag{34}$$

Here, the normal percent LOL at the rated HST of 110°C for a 24-hour operation is 0.0133% on the basis of the normal insulation life of 180000 hours [11].

The electricity supply is time-varying in power demands and nature. As a result, the transformer overload often occurs during the peak period of electric energy uses. However, the long-term overloading seriously affects the insulation life of transformer windings, and the transformer LOL should be controlled within a certain range, i.e. 0.0133% per 24 h. Generally, the transformer loading capability should be dynamically estimated from the transformer LOL [29]. An iterative flowchart to evaluate the dynamic loading capability of DBTS is illustrated in Fig. 6. After inputting the data of load factor, transformer parameters, ambient temperature and normal percent LOL, the HST of the buried transformer substation can be dynamically calculated by the proposed model in Fig.5 considering the underground heat

accumulative effect. Then, the %LOL can be determined based on the obtained HST. In the stage of dynamic loading capability evaluation, both of the %LOL at time t_i and the %LOL at prior operating periods should be considered to determine the load curtailment and increment, as shown in Fig.6. Consequently, the transformer load should be increased or decreased repeatedly to determine the maximum loading capacity of DBTS. For the end of each time cycle, the output data of %LOL, transformer load and HST should be exported for the next iterative time cycle.

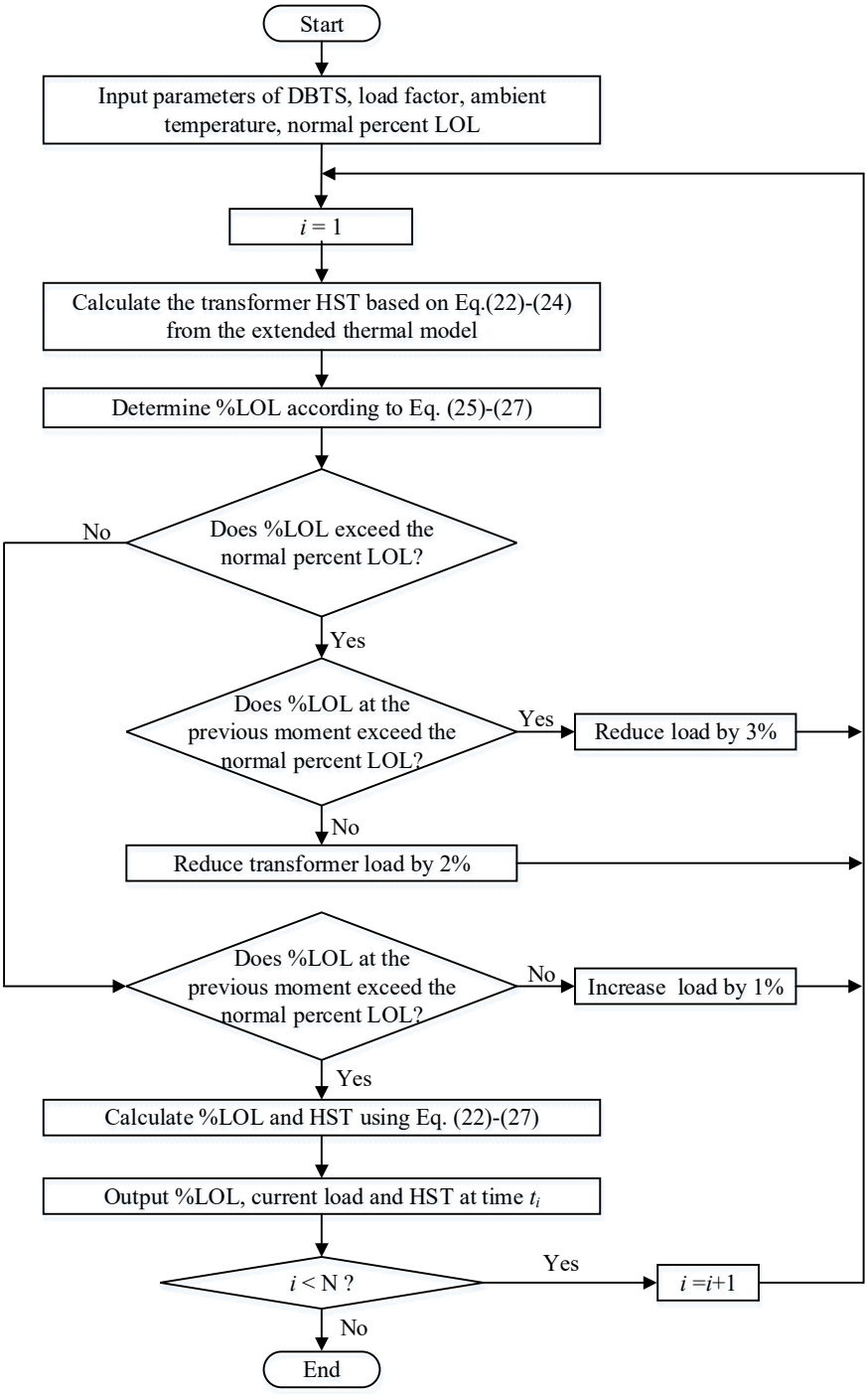

Fig. 6 Flowchart for dynamic loading capability evaluation based on the proposed model

IV. Case studies

A. Experimental Data and Settings

In this case study, a prefabricated substation with an oil-immersed power transformer S11-M.R.D-630 manufactured by Huaxiangxiangneng Electricity CO., LTD [36] is adopted for the finite element modelling and winding HST measurement. The sizes and rated power of DBTS components are tabulated in Table 6 and Table 7, respectively. The thermal properties of DBTS components and underground soil used to formulate the proposed thermal circuit model are summarized and listed in Table 8. Besides, the operating conditions for multi-point HST measurement are listed in Table 9. Fig. 7 and Fig. 8 show three-dimensional models of DBTS constructed using commercial computational fluid dynamics software packages ANSYS Icepak [41], respectively.

Table 6 Sizes of different DBTS components

Equipment	Length (mm)	Width (mm)	Height (mm)
DBTS enclosure	6000	2620	2520
Transformer tank	1060	458	970
Transformer base	-	-	100
Low-voltage boards	2400	600	2200
Medium-voltage cubicles	1500	800	2300

Table 7 Technical specifications of DBTS in the case study

Description	Value
Rated heat dissipation of Low-voltage boards (W)	332.7
Rated heat dissipation of Medium-voltage cubicles (W)	201.4
Rated voltage for primary transformer windings (kV)	10±2×2.5%
Rated voltage for secondary transformer windings (kV)	0.4
Rated capacity (kVA)	630
Transformer no-load loss (W)	810
Transformer load loss (W)	6200
Transformer no-load current (%)	0.6
Connection of transformer windings	Yyn0
Transformer short circuit impedance (%)	4.5

Table 8 Thermal properties of DBTS components and underground soil

Equipment (material)	Specific heat capacity ($J \cdot kg^{-1} \cdot K^{-1}$)	Thermal conductivity ($W \cdot m^{-1} \cdot K^{-1}$)	Density ($kg \cdot m^{-3}$)
Iron core (steel)	450	44	7500
Winding (cuprum)	390	385	8900
Transformer tank (iron)	500	45	7950
Soil	1645	1.8	1285
Transformer cooling fins (aluminium alloy)	600	150	3000
DBTS enclosure (galvanized steel sheet)	500	46	7800

Table 9 Experimental conditions of HST field-test measurement

Experimental items	Settings
Ambient temperature (℃)	13
Moisture concentration (%)	59
Atmospheric pressure (Pa)	88910
Experimental method	Short-circuit method
Measuring method	Thermocouple
Experimental duration	10 hour
Initial oil temperature (℃)	12
Load factor (p.u.)	0.8, 1.0 and 1.05
Start-up mode	Cold start

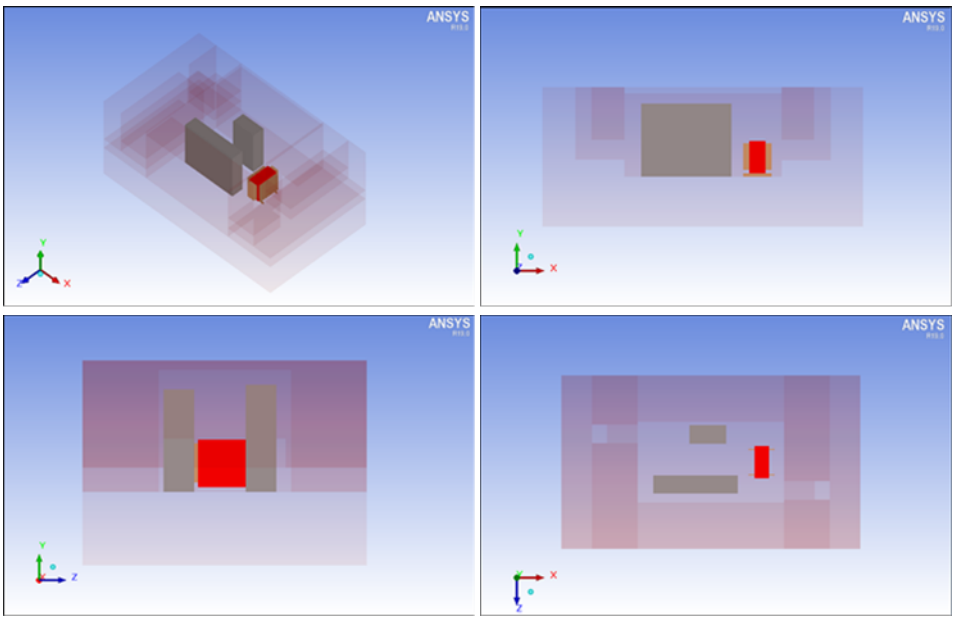

Fig. 7 Three-dimensional finite element model of DBTS using ANSYS Icepak

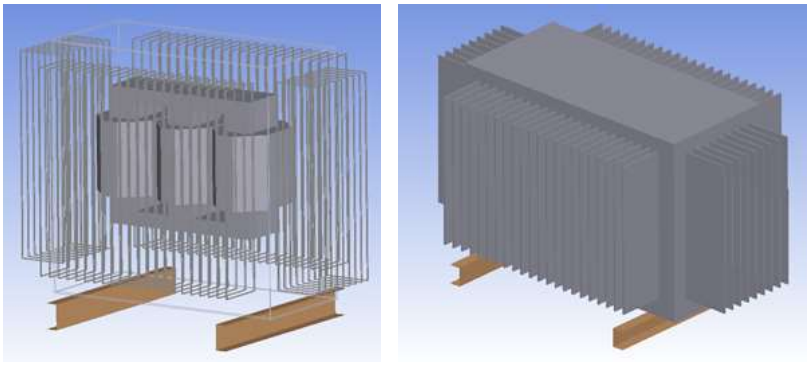

Fig. 8 Three-dimensional finite element model of the transformer using ANSYS Icepak

Fig. 9 and 10 provide the meshed finite element models of DBTS and its transformer using the software platform of ANSYS Icepak. In order to save the simulation time, the model built in ANSYS Icepak can be simplified by constructing these DBTS equipment with symmetrical hexahedral blocks, except for the transformer. Compared with the tetrahedral mesh, the hexahedral mesh has the lower special complexity and higher numerical accuracy [40]. As shown in Fig. 10, asymmetrical hexahedral meshes are applied to accommodate the non-uniform surfaces, such as transformer fins and their surroundings, and the intensive mesh generation is then used at the transformer region to obtain accurate numerical simulations. Due to large temperature gradient variations on the interfaces among the outer casing of DBTS, surrounding soils, the air and various devices in the substation, these interfaces between fluid and solid are drawn with multi-level meshes.

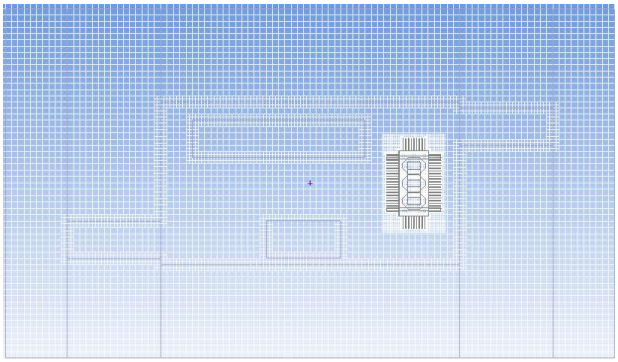

Fig. 9 Meshed finite element model of DBTS with ANSYS Icepak

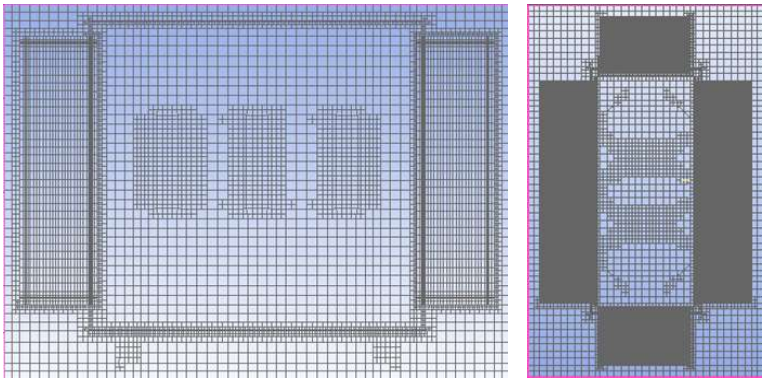

Fig. 10 Meshed finite element model of the transformer with ANSYS Icepak

Since the heat dissipation of transformer is mainly through the air natural convection, Boussinesq approximation is thus used to calculate the temperature field and fluid field inside the DBTS [9]. Based on the approximate Rayleigh number of 4.4862×10^{11} calculated by ANSYS Icepak, the flow regime in this paper is set as turbulent [40]. The radiant heat exchange has also been considered on the boundary between the substation enclosure and surrounding soils. Here, the boundary condition of soil ambient temperature is set to 13 °C. The ambient air pressure boundary condition is set to 101325 Pa, and a pressure boundary condition of 0 Pa is set at the ventilation hole outlet. The external pressure boundary conditions around the transformer are assumed to be symmetric.

The thermal finite-element analysis for the DBTS model under dynamic loading conditions requires the balance between simulation calculation efficiency and model accuracy. By adjusting the maximum and minimum allowable mesh sizes with different multi-level meshing settings, the cell numbers in the range from 1540000 to 5200000 can be obtained from the mesh generation process. Fig.11 shows the performance on the finite-element solution runtime and the average absolute error of dynamic HST calculation under the different number of cells. It is evident that the finite-element solution runtime increases dramatically with the improvement of model accuracy, and vice versa. A unique tradeoff between the solution runtime and model accuracy can be found on around 2900000 cells, and the results indicate that the further refinement of meshes has little effect on the model accuracy of finite-element simulations. Moreover, previous studies in [35] and [40] also employed the finite-element model with around 2000000 cells for thermodynamic analysis of transformer substations. Hence, the finite-element model of transformer is divided into 2360000 cells and 2600000 nodes in this study, and the settings with 2900000 cells are then formed for the finite-element model of the entire DBTS.

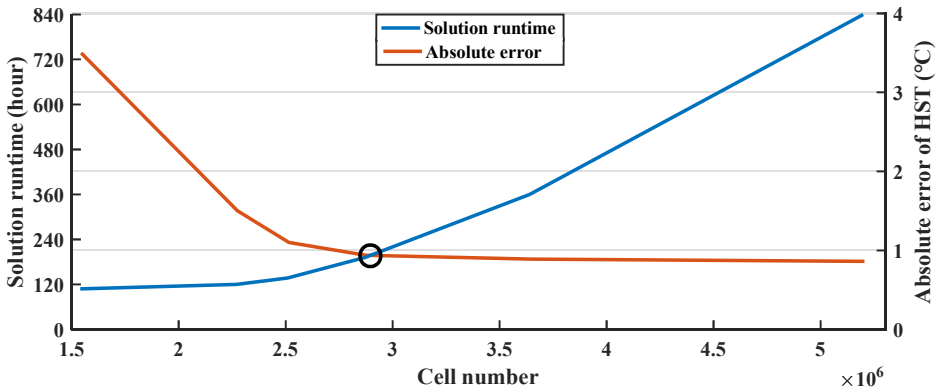

Fig. 11 Performances on solution runtime and HST deviation under different cell numbers

B. Tuning and Validation of Thermal Circuit Model

In this case study, the model parameters of the proposed thermal circuit, except for the soil thermal capacity and resistance, can be determined from Section II-C. Since the amount of soil involved in the heat dissipation is unidentified [38], the soil thermal resistance R_{earth} from Eq. (18)-(21) and the soil thermal capacity C_{earth} obtained from empirical values should be further tuned by the finite element analysis and multi-point HST measurement data. With the finite element model of DBTS using ANSYS Icepak, numerical simulations under the rated transformer load is implemented, and the temperature distribution results of the DBTS and its transformer are illustrated in Fig. 12 and Fig. 13, respectively.

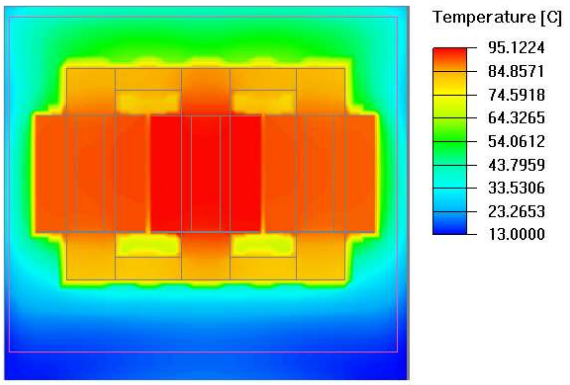

Fig. 12 Temperature distribution of transformer with finite element analysis

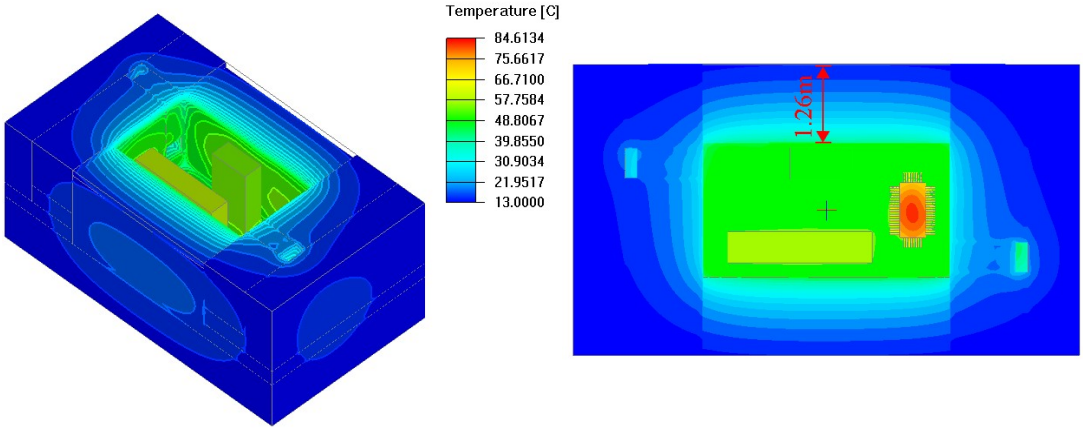

Fig. 13 Temperature distribution of DBTS with finite element analysis

As shown in Fig.12, for the three-phase transformer windings, the temperature of intermediate phase winding is slightly higher than those of other two phases due to its poor heat dissipation condition. It can also be found from Fig.13 that the temperature distribution of the soil surrounding the substation is uniform, and the soil temperature decreases with the increase of the distance from DBTS enclosure and ventilation channels. Moreover, it is observed that the soil temperature drops gradually to the ambient temperature 13 °C at the distance of about 1.26m from the DBTS enclosure, and thus the thickness of underground soils

involved in the heat transfer under the rated transformer loading can be obtained. Therefore, the parameters of soil thermal capacity and resistance are preliminarily determined by finite element analysis as listed in Table 10.

Table 10 Parameter settings of DBTS with finite element analysis

Parameters	L_{earth} (m)	Soil specific heat capacity (J kg^{-1} K^{-1})	Soil volume (m^3)
Value	1.26	1645	45.47

The preliminarily parameter settings of the proposed thermal model should further be tuned and verified by the measured field-test data provided by Huaxiangxiangneng Electricity CO., LTD [36]. The nonlinear least-squares method from Eq. (25)-(30) is used for the secondary tuning of DBTS model parameters, while the preliminarily parameter settings of DBTS can be used as the initial values of observation equation in Eq. (25).

The HST measurement experiment is performed with the experimental conditions in Table 9, and the measured HST data are obtained from temperature-dependent voltages produced by thermocouples [26]. Since the precise hot-spot location of transformer windings is difficult to determine beforehand [28], multi-point HST measurements on the transformer windings are implemented with six thermocouples. Based on finite element simulation results in Fig. 12, the hottest spot temperature shall be definitely located on the intermediate phase of three transformer windings due to the worst heat dissipation conditions, and then six thermocouples are installed at the phase B in the DBTS as shown in Fig. 14. The secondary tuning of DBTS parameters with measured data are listed in Table 11 after a large amount of comparative simulations.

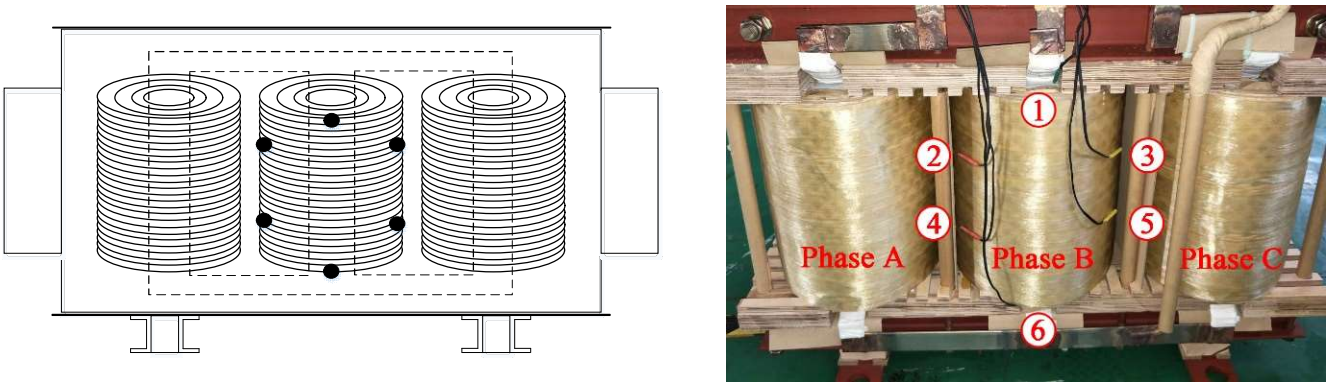

Fig. 14 Thermocouple locations for multi-point HST measurement

Table 11 Tuned parameter settings of DBTS with measured field-test data

Parameters	L_{earth} (m)	Soil specific heat capacity (J kg^{-1} K^{-1})	Soil volume (m^3)
Value	1.21	1632	43.18

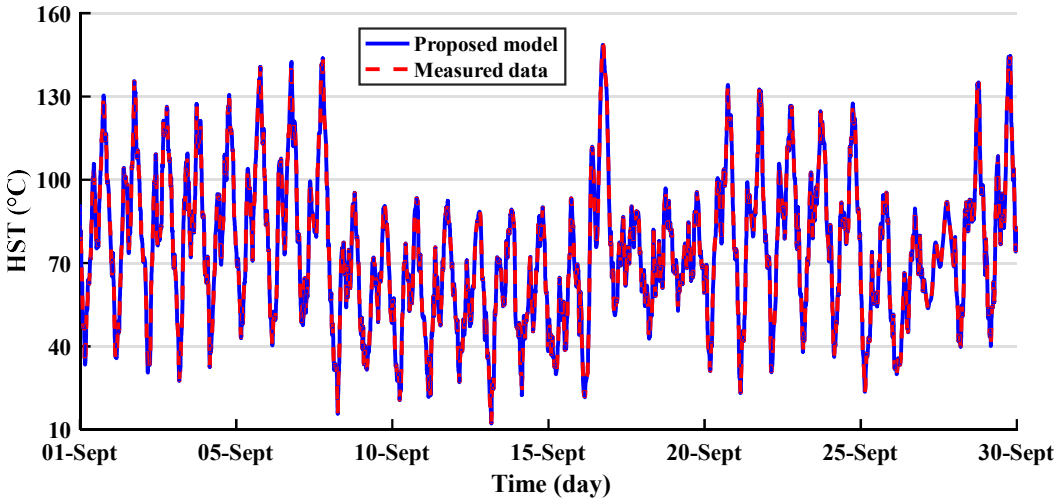

Fig. 15 Validation of the proposed thermal model with measured HST values in September 2017

With the tuned parameter settings of DBTS from Section II-C and Table 11, Fig. 15 illustrates the HST calculated by the proposed thermal circuit model and the measured data in September 2017 [36]. It should be noted that the ambient temperature in the thermal circuit model can be regarded as a varying ideal voltage source. It can be found that, the calculated HST from the proposed thermal model is closed with the measured values of HST, and thus the validation of the proposed thermal model can be confirmed. Consequently, the validity of the proposed thermal circuit model is verified by physical experiments and can be further used for transformer loading capacity evaluation.

C. Comparative Results and Discussions

In order to demonstrate the effectiveness and superiority of the proposed thermal circuit model, different methods for the transformer HST estimation, including basic thermal circuit model, finite element analysis and IEEE Loading Guide, are considered for further comparisons and analysis. Firstly, Fig. 16 illustrates the measured temperature curves of transformer windings under the load factor of 1.05, and these data are extracted from multi-point measurements of thermocouples as shown in Fig. 14. It can be found that the measured temperature exhibits a certain fluctuation, and the measuring point 2 shows the highest temperature and thus is selected as the hottest hot-spot for further model analysis. In this study, the average values of the hottest HST from the measuring point 2, represented by the bright yellow solid line in Fig. 16, is taken as the measured benchmarking data of transformer HST.

Fig. 17 illustrates the HST results obtained from different methods under load factors of 0.8, 1.0 and 1.05. The validity of the finite element model is checked by comparing the HST obtained from the finite element analysis with the experimentally measured data, obtaining acceptable differences of only -0.52°C,

-0.6℃ and -0.94℃ under different loading conditions. It is evident that the HST curve determined by the proposed thermal circuit model is closed to the measured data, especially during the stable period. Because of the lack of consideration for underground heat accumulative effect, both of HST results calculated with IEEE Loading Guide and basic thermal model rise rapidly and significantly higher than the measured data especially during the rising period in Fig. 17. Compared with the calculation model in IEEE Loading Guide [11], the HST values from the proposed model can be improved by 0.78℃, 1.65℃ and 1.94℃ under different loading conditions, respectively. Furthermore, it can be found that the improved calculation accuracy of the proposed model increases with the transformer load growth, because the heat accumulative effect becomes more significant as the HTS increases.

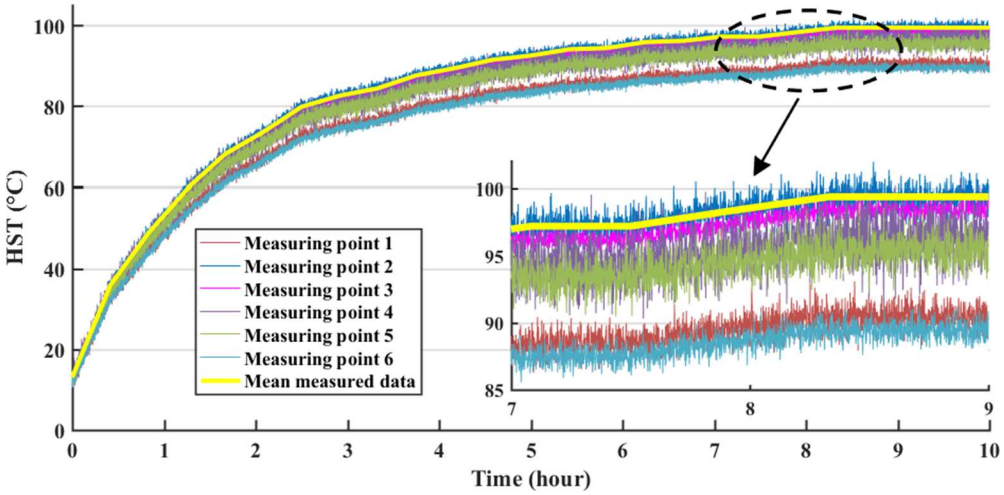

Fig. 16 Treatment of temperature fluctuations from multi-point measurements

A typical daily transformer load provided by Huaxiangxiangneng Electricity CO., LTD in [36] is used to demonstrate dynamic HST calculations, as shown in Fig. 18. Since the load demand changes rapidly in the peak-load period, the accurate estimation for the winding HST is important for dynamic assessment of transformer loading capability. Fig. 19 compares the obtained HST results with different methods during the peak-load period from 16:30 pm to 19:30 pm. It can be found from Fig. 19 that, with the underground heat accumulative effect, the transformer HST rises slowly as the load grows rapidly during the peak-load period, and therefore the HST curves obtained by the proposed model and finite element analysis are closed to the measured data for the improved HST estimation accuracy. In this study, simulations are performed on a workstation Dell Precision T7920, with 8-core 16-thread 2.1 GHz Intel Xeon Gold processor and 128 GB of RAM. It can be found from ten independent runs of finite element simulations that, the solution runtime of a single finite element simulation under the steady transformer loading for the cold-start HST calculation is ranged from 4 to 6 hours, and the average runtime is approximately 4.8 hours. Furthermore,

it should be noted from Fig. 11 that, the finite element analysis needs to spend more than 179 hours for the dynamic HST calculation under the peak-load period due to the large number of hexahedral cells and the complicated solution processes of partial differential equations. The proposed model only requires a few seconds for estimating the HST under various loading conditions, and therefore can readily satisfy the time requirement of real-time transformer load management.

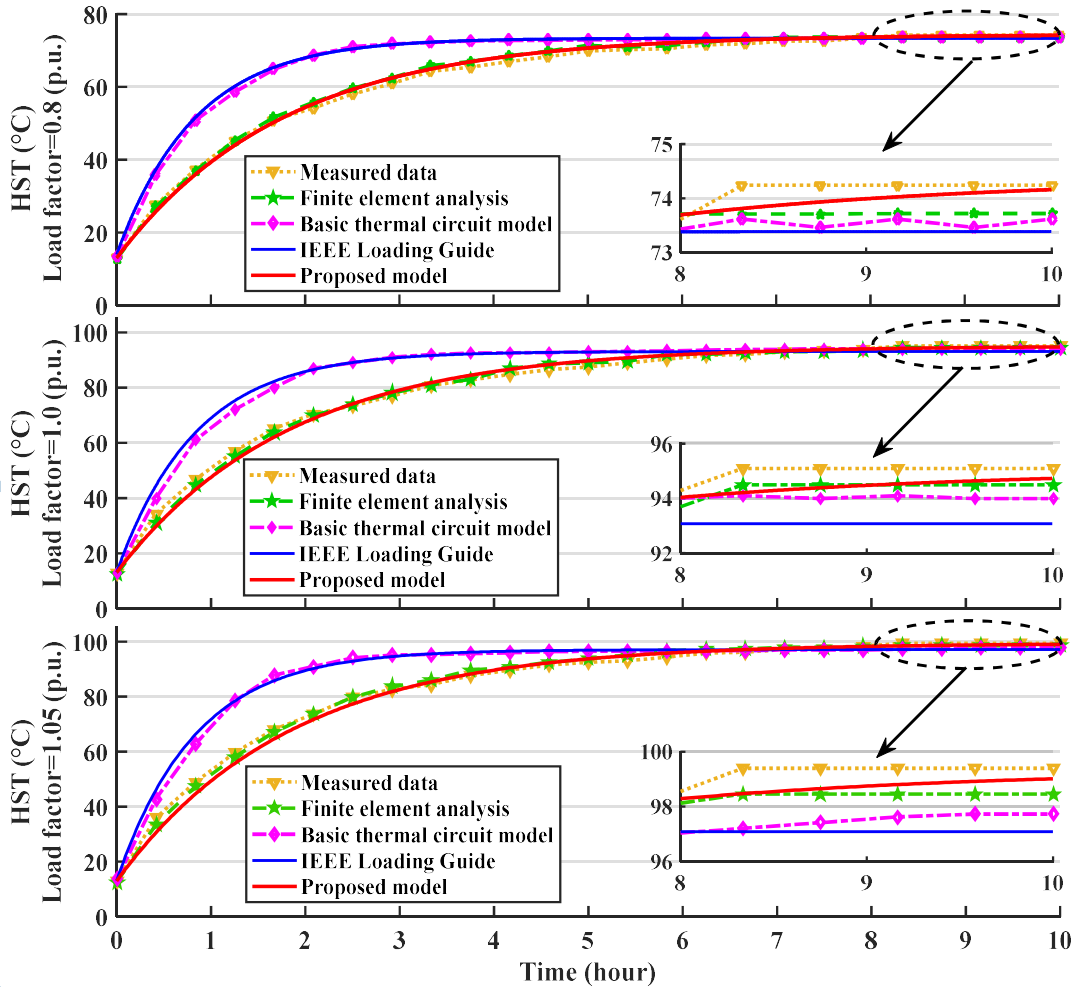

Fig. 17 Comparative HST results response to a cold start under different load factors

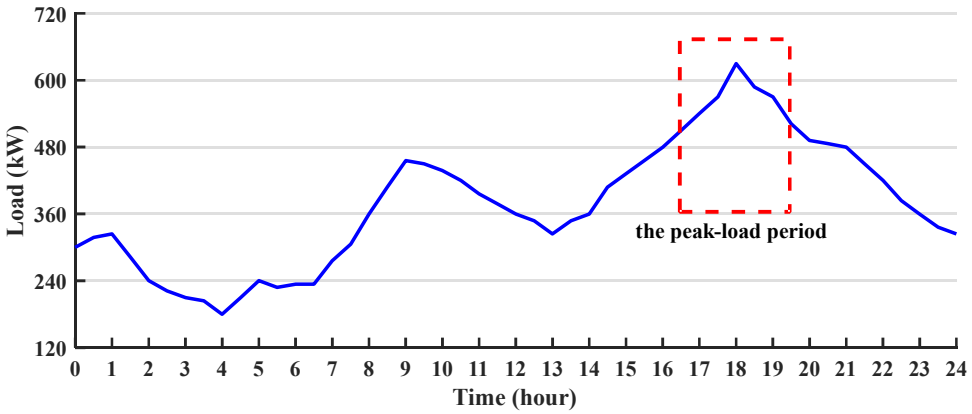

Fig. 18 Typical daily transformer load

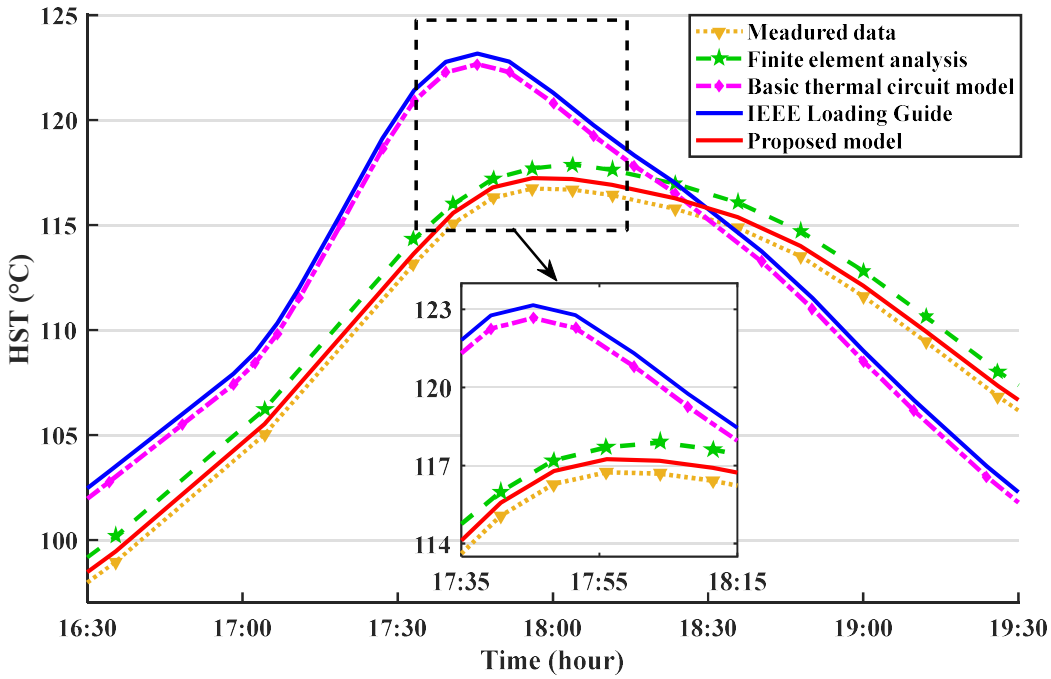

Fig. 19 Comparative HST results during peak-load period

Fig. 20 shows the evaluation results of dynamic transformer loading capability based on the iterative calculation flowchart in Section III-B. It is clear that the transformer loading capability will decrease with the rise on HST, and the minimum loading capability points correspond to the maximum HSTs. In addition, due to the temperature lag caused by the soil thermal dissipation properties, the transformer loading capability determined by the proposed model significantly higher than the results from other methods, and the method in IEEE Loading Guide underestimates the dynamic loading capability. Therefore, during the peak-load period, the proposed thermal circuit model can increase the dynamic loading capability by 12.17% compared with IEEE Loading Guide.

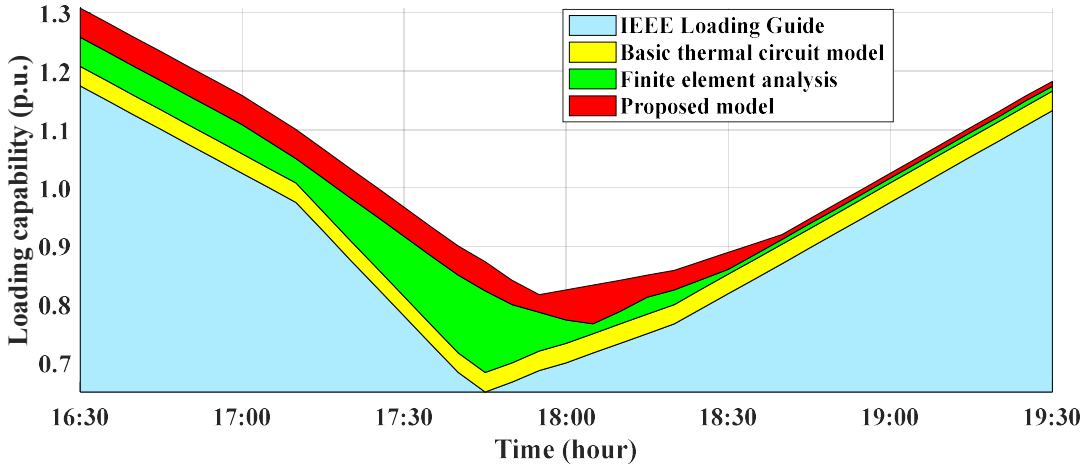

Fig. 20 Dynamic loading capability during peak-load period

Fig. 21 compares the transformer LOL results caused by overloading and high HSTs using different methods during peak-load period. It can be found that, compared with IEEE Loading Guide, the proposed model can substantially decrease the transformer LOL, and hence can effectively extend the transformer's life cycle. Moreover, based on Eq. (31)-(34), comparative statistical performance results obtained with the proposed model and the other three methods under the typical daily load are listed in Table 12. It is obvious that the proposed model can provide superior performance on the HST estimation accuracy, dynamic loading capability, and transformer LOL reduction. It should be noted from the statistical performance results that, compared with the method in IEEE Loading Guide, the proposed model can reduce the transformer LOL by 15.67% and extend the transformers lifetime cycle by 18.59%.

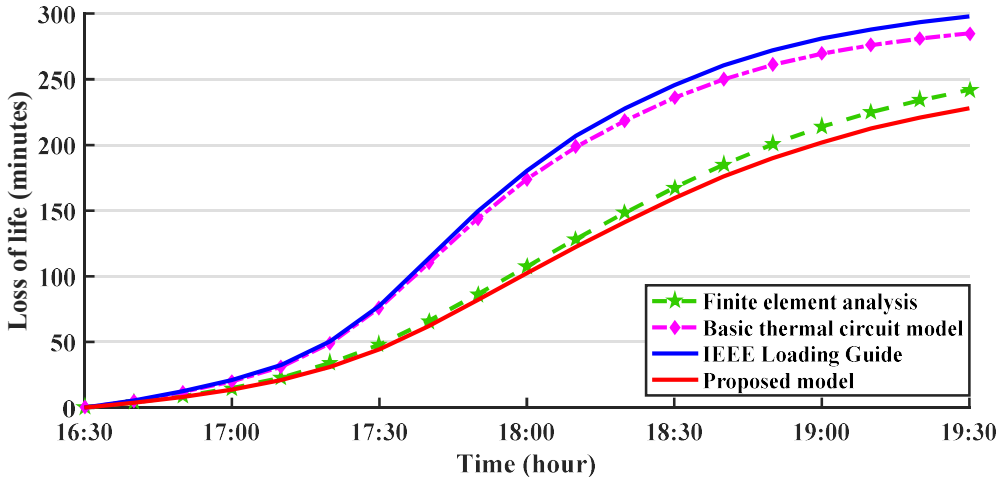

Fig. 21 Transformer LOL during peak-load period

Table 12 Comparative performance results under a typical daily load

Methods	Proposed model	IEEE Loading Guide	Finite elment analysis	Basic thermal circuit model
Mean absolute error of HST (°C)	**0.42**	3.78	0.89	3.32
HST estimation accuracy (%)	**99.25**	91.90	98.21	92.14
Dynamic loading capability (p.u.)	**1.352**	1.339	1.348	1.343
LOL time (minute)	**371.73**	440.82	382.55	412.78
Transformer lifetime expectancy (hour)	**213462**	180000	207414	192222

V. Conclusions

In this paper, the problems of temperature rise and heat dissipation of DBTS are studied, and an extended thermal circuit model for direct-buried transformer considering the underground heat accumulative effect is proposed to dynamically evaluate the transformer loading capability. The conclusions of this investigation are summarized as follows: 1) The underground heat accumulative effect has been discovered to have a significant thermal lags impact on the transformer HST in the fully buried transformer substation; 2) The validation of the extended thermal circuit model considering soil thermal properties has been confirmed by the field-test measured data, and the HST estimation accuracy can be improved by 7.35% and 7.11% compared with IEEE Loading Guide and basic thermal circuit model, respectively; 3) Compared to the method in IEEE Loading Guide, the proposed thermal circuit model can significantly improve the dynamic loading capability, and prolong the life expectancy of direct-buried transformers by 18.59%. Further on-going research will focus on the dynamic loading capability assessment for the parallel operation of multiple direct-buried transformers.

Acknowledgment

This work was jointly supported by the Research Grants Council of the HKSAR Government (Grant No. R5020-18), the Innovation and Technology Commission of the HKSAR Government to the Hong Kong Branch of National Rail Transit Electrification and Automation Engineering Technology Research Center (Grant No. K-BBY1), the National Natural Science Foundation of China (51877072), and Huxiang Young Talents programme of Hunan Province under Grant 2019RS2018.

References

[1] UN Habitat. World Cities Report 2016: Urbanization and development-emerging futures. Available from: https://unhabitat.org/books/world-cities-report/

[2] Fuentes G J, Galaktionov O, Bermudez C. Special urban transformer substation. The 19st CIRED International Conference on Electricity Distribution, Vienna, Austria, 21-24 May, 2007, pp. 1-4.

[3] El-Fouly T H M, Zeineldin H H, El-Saadany E F, Salama M M A. A new optimization model for distribution substation siting, sizing, and timing. International Journal of Electrical Power & Energy Systems, 2008, 30(5): 308-315.

[4] Sadovskaia K, Bogdanov D, Honkapuro S, Breyer C. Power transmission and distribution losses–A model based on available empirical data and future trends for all countries globally. International Journal of Electrical Power & Energy Systems, 2019, 107: 98-109.

[5] Huss A, Goris K, Vermeulen R, Kromhout H. Does apartment's distance to an in-built transformer room predict magnetic field exposure levels? Journal of Exposure Science and Environmental Epidemiology, 2013, 23(5): 554-558.

[6] Groot D F, Riet V M, Buisman G. The full underground distribution transformer in practice. The 21st CIRED International Conference on Electricity Distribution, Frankfurt, Germany, 6-9 June, 2011, pp. 1-4.

[7] Sandraz J P A, De Leon F, Cultrera J. Validated transient heat-transfer model for underground transformer in rectangular vault. IEEE Transactions on Power Delivery, 2013, 28(3): 1770-1778.

[8] Beiza M, Ramos J C, Rivas A, et al. Zonal thermal model of the ventilation of underground transformer substations: Development and parametric study. Applied Thermal Engineering, 2014, 62(1): 215-228.

[9] Ramos J C, Beiza M, Gastelurrutia M, et al. Numerical modelling of the natural ventilation of underground transformer substations. Applied Thermal Engineering, 2013, 51: 852-863.

[10] Zhang N, Wang Z. Review of soil thermal conductivity and predictive models. International Journal of Thermal Sciences, 2017, 117: 172-183.

[11] IEEE Guide for Loading Mineral-Oil-Immersed Transformers and Step-Voltage Regulators. IEEE Std C57.91-2011 (Revision of IEEE Std C57.91-1995), March, 2012.

[12] Christina A J, Salam, M A, Rahman Q M, et al. Causes of transformer failures and diagnostic methods-A review. Renewable and Sustainable Energy Reviews, 2018, 82: 1442-1456.

[13] Krishnamurthy S, Baningobera B E. IEC61850 standard-based harmonic blocking scheme for power transformers. Protection and Control of Modern Power Systems, 2019, 4(4): 121-135.

[14] Villacci D, Bontempi G, Vaccaro A, Birattari M. The role of learning methods in the dynamic assessment of power components loading capability. IEEE Transactions on Industrial Electronics, 2005, 52(1): 280-290.

[15] Djamali M, Tenbohlen S, Junge E, Konermann M. Real-time evaluation of the dynamic loading capability of indoor distribution transformers. IEEE Transactions on Power Delivery, 2017, 33(3): 1134-1142.

[16] Gouvea M R, Robba E J, Belvedere E C, et, al. Thermal simulation for distribution transformers in underground vaults. 2004 IEEE/PES Transmission and Distribution Conference and Exposition: Latin America, Sao Paulo, Brazil, 8-11 November, 2004, pp. 1-5.

[17] Frey L T. Direct buried transformer thermal evaluation. IEEE Transactions on Power Apparatus and Systems, 1972, 3: 959-968.

[18] Swift G, Molinski T S, Lehn W. A fundamental approach to transformer thermal modeling. I. Theory and equivalent circuit. IEEE Transactions on Power Delivery, 2001, 16(2): 171-175.

[19] Iskender I, Mamizadeh A. An improved nonlinear thermal model for MV/LV prefabricated oil-immersed power transformer substations. Electrical Engineering, 2011, 93(1): 9-22.

[20] Mamizadeh A, Iskender I. Analyzing and comparing thermal models of indoor and outdoor oil-immersed power transformers. 2009 IEEE Bucharest PowerTech. Bucharest, Romania 28th June- 2nd July, 2009. pp. 1-6.

[21] Abdelsamad S F, Morsi W G, Sidhu T S. Probabilistic impact of transportation electrification on the loss-of-life of distribution transformers in the presence of rooftop solar photovoltaic. IEEE Transactions on Sustainable Energy, 2015, 6(4): 1565-1573.

[22] Chen C S, Ku T T, Lin C H. Implementation of a systematic distribution transformer load management in Taipower. IET Generation, Transmission & Distribution, 2009, 3(3): 286-295.
[23] Okabe S, Yamada M, Nojima K, Suzuki K. Transient response of a grounding system in an underground GIS substation. Electrical Engineering in Japan, 2004, 146(1): 70-77.
[24] Sun W, Yang L, Zare F, et al. Improved method for aging assessment of winding hot-spot insulation of transformer based on the 2-FAL concentration in oil. International Journal of Electrical Power & Energy Systems, 2019, 112: 191-198.
[25] Niu W, Zhang G, Jiang Y, et, al. The experimental study of a novel cooling system of a power transformer in an urban underground substation. 2010 International Conference on Power System Technology, Hangzhou, China, 24-28 October, 2010, pp. 1-6.
[26] Ribeiro A L, Eira N F, Sousa J M, et al. Multipoint fiber-optic hot-spot sensing network integrated into high power transformer for continuous monitoring. IEEE Sensors Journal, 2008, 8(7): 1264-1267.
[27] Tang W H, Wu Q. H, Richardson Z J. A simplified transformer thermal model based on thermal-electric analogy. IEEE Transactions on Power Delivery, 2004, 19(3): 1112-1119.
[28] Lachman M F, Griffin P J, Walter, W, Wilson A. Real-time dynamic loading and thermal diagnostic of power transformers. IEEE Transactions on Power Delivery, 2003, 18(1): 142-148.
[29] Taheri S, Gholami A, Fofana I, et al. Modeling and simulation of transformer loading capability and hot spot temperature under harmonic conditions. Electric Power Systems Research, 2012, 86: 68-75.
[30] Susa D, Lehtonen M, Nordman H. Dynamic thermal modelling of power transformers. IEEE Transactions on Power Delivery, 2005, 20(1): 197-204.
[31] Susa D, Nordman H. A simple model for calculating transformer hot-spot temperature. IEEE Transactions on Power Delivery, 2009, 24(3): 1252-1265.
[32] Radakovic Z, Jevtic M, Das B. Dynamic thermal model of kiosk oil immersed transformers based on the thermal buoyancy driven air flow. International Journal of Electrical Power & Energy Systems, 2017, 92: 14-24.
[33] Radakovic Z, Maksimovic S. Non-stationary thermal model of indoor transformer stations. Electrical Engineering, 2002, 84(2): 109-117.
[34] Degefa M Z, Millar R J, Lehtonen M and Hyvonen P. Dynamic Thermal Modeling of MV/LV Prefabricated Substations. IEEE Transactions on Power Delivery, 2014, 29(2): 786-793.
[35] Santisteban A, Delgado F, Ortiz A, et al. Numerical analysis of the hot-spot temperature of a power transformer with alternative dielectric liquids. IEEE Transactions on Dielectrics and Electrical Insulation, 2017, 24(5): 3226-3235.
[36] Huaxiangxiangneng Electricity CO., LTD. Technical report on the development and industrialization of intelligent buried transformer substations (in Chinese), Rep. No. 722528827-2016GK2105-01, 2018. Available from: http://www.hxxncorp.com/index.php?m=content&c=index&a=show&catid=47&id=101
[37] Xu D, Wu Q, Zhou B, et al. Distributed multi-energy operation of coupled electricity, heating and natural gas networks. IEEE Transactions on Sustainable Energy, DOI: 10.1109/TSTE.2019.2961432, 2020.

[38] Lu S, Ren T, Gong Y, Horton R. An improved model for predicting soil thermal conductivity from water content at room temperature. Soil Science Society of America Journal, 2007, 71(1): 8-14.
[39] Naranjo-Mendoza C, Wright A, Oyinlola M, Greenough R. A comparison of analytical and numerical model predictions of shallow soil temperature variation with experimental measurements. Geothermics, 2018, 76: 38-49.
[40] Gastelurrutia J, Ramos J, Larraona G, et al. Numerical modelling of natural convection of oil inside distribution transformers. Applied thermal engineering, 2011, 31(4): 493-505.
[41] Madenci E, Guven I. The finite element method and applications in engineering using ANSYS®. Springer, 2015.